Bulk and surface properties of metals by full-charge-density screened Korringa-Kohn-Rostoker calculations

J. Zabloudil,[1] R. Hammerling,[1] L. Szunyogh,[1,2] and P. Weinberger[1]
[1]*Center for Computational Material Science, Vienna University of Technology, Getreidemarkt 9/134, A-1060 Vienna, Austria*
[2]*Department of Theoretical Physics and Center for Applied Mathematics and Computational Physics, Budapest University of Technology and Economics, Budafoki út 8, H-1521 Budapest, Hungary*
(Received 26 July 2005; revised manuscript received 19 January 2006; published 14 March 2006)

The full-charge-density screened Korringa-Kohn-Rostoker method is described and applied to calculate bulk and surface energies of transition metals. It is demonstrated that due to a truncated angular momentum expansion of the shape functions, the otherwise ultimate freedom of adding a constant to the potential in all space leads, in particular close to the cell boundaries, to potentials of fairly different shapes. Thus a dependence on this constant potential shift emerges for the calculated bulk total energies, equilibrium volumes, and bulk moduli, as well as for the surface energies and the work functions. A reasonable choice for the constant shift seems to set the bulk potential at the muffin-tin radius to zero. By making this choice the calculations give results that are in very good agreement to those calculated by other full-charge-density or full-potential methods.

DOI: 10.1103/PhysRevB.73.115410 PACS number(s): 71.15.Ap, 71.15.Nc

I. INTRODUCTION

In order to remove deficiencies of the atomic sphere approximation (ASA) one would like to describe the potentials and the charge (and magnetization) densities in such a way that nonspherical contributions in the interstitial region (and to some extent even inside the nonoverlapping muffin tins) are described correctly. Such a description is in principle provided by a full-potential (FP) approach which has already been implemented and used in various methods of electronic structure calculation. The main drawback of this approach is the disproportional computation time compared to the gain in accuracy achieved by using a complete FP description. In recent years a technique has come up which requires the knowledge of just the spherically symmetric part of the potential while still making use of the full nonspherically symmetric charge distribution; hence, it is called the *full-charge-density* (FCD) method.[1–4] It turned out that results obtained from such a technique compare very well to those of FP methods. The main reason for this is that it is more crucial to calculate the total energy of the system by taking into account the anisotropic charge density (even from a spherical potential) than to evaluate the self-consistent anisotropic potential. Another point is that FP methods have to be used for a certain $\ell_{\max}$ in order to be practically applicable. Usually $\ell_{\max}=3$ is used for the radial amplitudes, in certain cases even $\ell_{\max}=4$, implying that for the potential and charge density an $\ell_{\max}=6$ or $\ell_{\max}=8$ has to be considered. Since in order to account for the nonspherical shape of the Wigner-Seitz cells multiple-scattering-based FP methods [Korringa-Kohn-Rostoker (KKR), linear muffin-tin orbital (LMTO)] make use of shape functions which are slowly converging in angular momentum space, the convergence against $\ell_{\max}$ should carefully be checked in these types of calculations. It should be mentioned that intra-atomic forces needed to perform geometry optimization can be calculated accurately only by using a truly FP scheme—i.e., by taking into account the nonspherical components of the potential.

In the following we shall discuss a full-charge-density technique as implemented within the screened Korringa-Kohn-Rostoker (SKKR) method[5] (in the following referred to as the FCD-SKKR method). It relies on using only the spherically symmetric part of the single-cell potential for finding the scattering solutions of the Schrödinger (or Dirac) equation, describing, however, the highly nonspherically symmetric charge density in the interstitial region correctly. The major gain is an accurate computation of total energies while keeping the efficiency of the ASA. In what follows we outline the main features of this method and present results for the bulk and surface properties of transition metals.

In using the FCD-SKKR method we faced, however, the following problem. In the case of an exact solution of the Schrödinger and Poisson equations one has the freedom to add a constant "shift" to the potential that leaves the total energy of the system unchanged. As will be demonstrated, due to truncations in angular momentum space used for the shape functions the invariance of the results with respect to

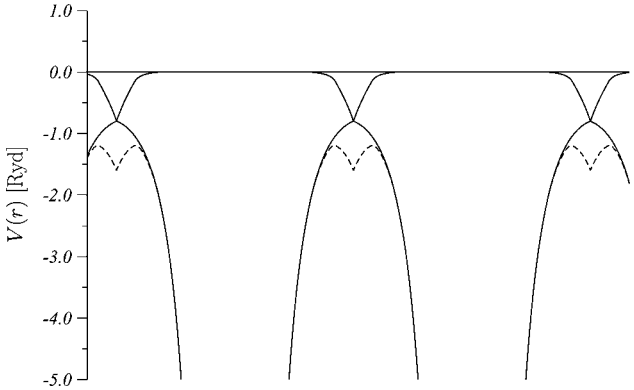

FIG. 1. $v_{00}(r)/\sqrt{4\pi}$ (solid line) and the resulting full-crystal potential (dashed line) for fcc Cu along a nearest-neighbor direction. The potential is shifted to −0.8 Ry at the muffin-tin radii.

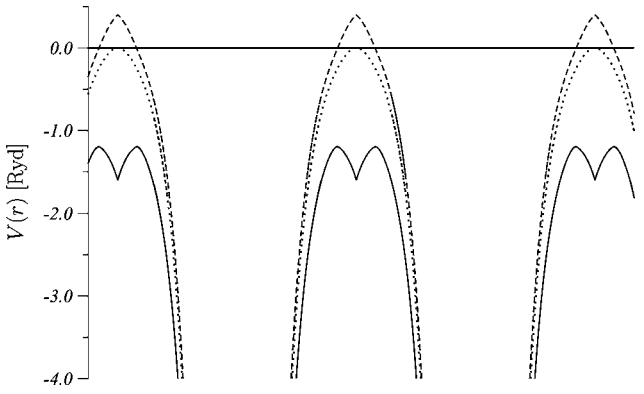

FIG. 2. Full-crystal potential for Cu bulk in the nearest-neighbor direction for different shift parameters. Solid line: $V_{\mathrm{MT}}=-0.8$ Ry. Dashed line: $V_{\mathrm{MT}}=+0.2$ Ry. Dotted line: $V_{\mathrm{MT}}=0.0$ Ry.

an arbitrary shift of the potential is not satisfied. By the way, such a dependence is also found when using the ASA. We present systematic calculations as a function of the potential shift and conclude that, at least for the case of simple lattices, a reasonable choice for this potential shift can be made that reproduces well the results obtained by other FCD or FP methods.

II. SINGLE-SITE PROBLEM

The full-crystal potential denoted by $V(\mathbf{r})$ can be expanded around the position vector pointing to the center of cell i (center of the corresponding Wigner-Seitz cell), $\mathbf{R}_i$, in terms of complex spherical harmonics[6] as

$$V(\mathbf{r}) = \sum_L V_{iL}(r_i) Y_L(\hat{\mathbf{r}}_i), \quad \mathbf{r}_i = \mathbf{r} - \mathbf{R}_i, \tag{1}$$

where $L=(\ell,m)$ denotes a composite angular momentum index. The potential $V(\mathbf{r})$ can be written as a sum of individual potentials confined to space-filling Wigner-Seitz cells,

$$V(\mathbf{r}) = \sum_i v_i(\mathbf{r}), \tag{2}$$

where the single-cell potential $v_i(\mathbf{r})$ can be expressed by using shape functions[7–9] $\sigma_i(\mathbf{r})$ that project to the respective Wigner-Seitz polyhedron, Ω_i,

$$\sigma_i(\mathbf{r}) = \begin{cases} 1 & \text{if } \mathbf{r} \in \Omega_i, \\ 0 & \text{anyway}, \end{cases} \tag{3}$$

$$\sigma_i(\mathbf{r}) = \sum_L \sigma_{iL}(r_i) Y_L(\hat{\mathbf{r}}_i), \tag{4}$$

as

$$v_i(\mathbf{r}) = V(\mathbf{r}) \sigma_i(\mathbf{r}). \tag{5}$$

The single-site potential $v_i(\mathbf{r})$ can now be expanded in terms of complex spherical harmonics,

$$v_i(\mathbf{r}) = \sum_L v_{iL}(r_i) Y_L(\hat{\mathbf{r}}_i), \tag{6}$$

where the expansion coefficients are given by

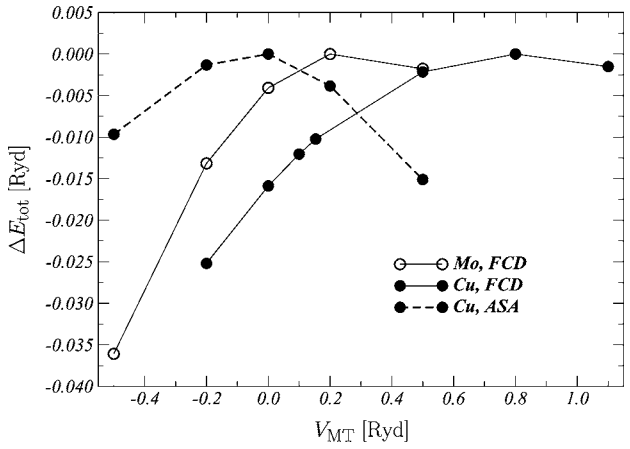

FIG. 3. Relative change of the total energy, $\Delta E_{\mathrm{tot}}=E_{\mathrm{tot}}-E_{\mathrm{tot}}^{\mathrm{max}}$, of bulk Cu and Mo with respect to the potential at the muffin-tin radius, V_{MT}.

$$v_{iL}(r_i) = \sum_{L'L''} C^L_{L'L''} V_{iL'}(r_i) \sigma_{iL''}(r_i), \tag{7}$$

with the Gaunt coefficients, $C^L_{L'L''}$, defined by

$$C^L_{L'L''} = \int \mathrm{d}\hat{\mathbf{r}} Y_L(\hat{\mathbf{r}})^* Y_{L'}(\hat{\mathbf{r}}) Y_{L''}(\hat{\mathbf{r}}). \tag{8}$$

In a full-potential method the single-site problem should be solved for the anisotropic potential $v_i(\mathbf{r})$; see Eq. (6). The anisotropy in this case not only arises from the aspherical shape of the potential $V(\mathbf{r})$, but also from the shape function $\sigma_i(\mathbf{r})$. To simplify the single-site problem we use only the spherical component of this "shape-truncated" potential, $v_{i,00}(r_i)Y_{00}(\hat{\mathbf{r}}_i)=v_{i,00}(r_i)/\sqrt{4\pi}$. Then the potential entering the Schrödinger equation is given by

$$\frac{1}{\sqrt{4\pi}} v_{i,00}(r_i) = \frac{1}{4\pi} \sum_L V_{iL}(r_i) \sigma_{iL}(r_i), \tag{9}$$

which is the so-called "zeroth approximation" to a full potential. Furthermore, if only the spherically symmetric component of the crystal potential is taken into account, we have

$$v_i^0(r_i) = \frac{1}{4\pi} V_{i,00}(r_i) \sigma_{i,00}(r_i). \tag{10}$$

Whether one takes the potential of Eq. (9) or that of Eq. (10) turns out to be of minor importance for the quantities presented in Sec. VI.

III. CONSTANT POTENTIAL "SHIFT"

Within density functional theory[10] one is in principle free to add a constant value V^{c} to the full (crystal) potential $V(\mathbf{r})$,

$$\tilde{V}(\mathbf{r}) = V(\mathbf{r}) + V^{\mathrm{c}} \tag{11}$$

$$= \sum_i [v_i(\mathbf{r}_i) + \sigma_i(\mathbf{r}_i) V^{\mathrm{c}}], \tag{12}$$

since in a self-consistent (converged) full-potential calculation the results should be independent of such a constant.

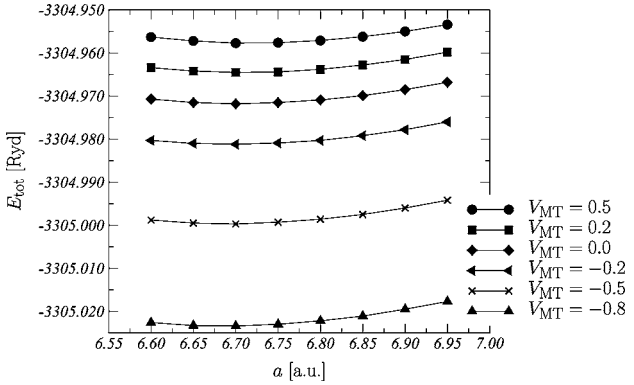

FIG. 4. Total energy of bulk Cu as a function of the lattice constant a for different values of the potential at the muffin-tin radius, V_{MT} (in rydberg units).

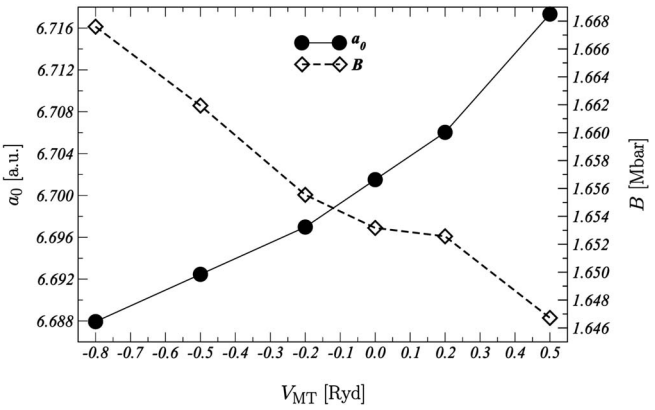

FIG. 5. Equilibrium lattice parameter a_0 and bulk modulus B of bulk Cu as a function of the potential at the muffin-tin radius, V_{MT}.

However, in practical terms—i.e., by using truncated angular momentum expansions—the final self-consistent potential as well as the charge density and subsequently also the total energy do depend on the choice of V^c. In Fig. 1 the crystal potential of Cu as constructed from spherical single-cell potentials, Eq. (9), is shown along a nearest-neighbor direction. Note that the boundaries of the adjacent cells correspond to the muffin-tin radius r_{MT}. For the case displayed in Fig. 1 we have chosen a potential shift V^c such that the single-site potential at r_{MT}, V_{MT}, equals −0.8 Ry. As can be seen, the individual potentials are not exactly confined to the corresponding Wigner-Seitz cells but have "tails" that go smoothly to zero beyond r_{MT}. If these overlapping potentials are added up, a local minimum with a discontinuous derivative appears at the boundary of neighboring cells. Furthermore, the ultimate relationship between the full-crystal and the single-cell potentials [see Eq. (5)] is not satisfied.

By varying the potential shift V^c, different shapes for the full-crystal potential are obtained as is evident from Fig. 2. From this figure it is also obvious that the condition in Eq. (5) is best satisfied for the case of $V_{MT}=0$. It should be noted that by using spherical potentials this condition is exactly satisfied only for nonoverlapping muffin-tin potentials—i.e., when $v_i(r_i)=0$ for $r_i > r_{MT}$.

The existence of this parameter has been noted previously by other authors from a slightly different viewpoint.[4,11] In Refs. 4 and 11 some suggestions for the best choice of V^c as summarized below are given:

$$V^{c,(1)} = \langle V \rangle_{\Omega_{\text{WS-MT}}} = \int_{r_{MT}}^{r_{BS}} r^2 \mathrm{d}r \sum_L V_L(r)\sigma_L(r)/\Omega_{\text{WS-MT}}, \tag{13}$$

$$V^{c,(2)} = \langle V \rangle_{\Omega_{\text{BS-MT}}} = \sqrt{4\pi} \int_{r_{MT}}^{r_{BS}} r^2 \mathrm{d}r V_{00}(r)/\Omega_{\text{BS-MT}}, \tag{14}$$

$$V^{c,(3)} = \frac{\langle \rho V \rangle_{\Omega_{\text{WS-MT}}}}{\langle \rho \rangle_{\Omega_{\text{WS-MT}}}} = \int_{r_{MT}}^{r_{BS}} r^2 \mathrm{d}r \sum_{LL'L''} C^L_{L'L''} \rho_L(r) V_{L'}(r) \sigma_{L''}(r) / \int_{r_{MT}}^{r_{BS}} r^2 \mathrm{d}r \times \sum_L \rho_L(r)\sigma_L(r), \tag{15}$$

$$V^{c,(4)} = \frac{\langle \rho V \rangle_{\Omega_{\text{BS-MT}}}}{\langle \rho \rangle_{\Omega_{\text{BS-MT}}}} = \int_{r_{MT}}^{r_{BS}} r^2 \mathrm{d}r \sum_L V_L(r)\rho_L(r)/\sqrt{4\pi} \int_{r_{MT}}^{r_{BS}} r^2 \mathrm{d}r \rho_{00}(r). \tag{16}$$

As can be seen from these expressions the main idea is to take the average of the potential or the potential weighted by the charge density, $\rho(\mathbf{r})$, in the interstitial region. The interstitial region may either be defined as the difference of the volumes of the Wigner-Seitz cell and the muffin-tin sphere ($\Omega_{\text{WS-MT}}$) or, alternatively, of the bounding sphere and muffin-tin sphere ($\Omega_{\text{BS-MT}}$). Values for V_{MT} using shift parameters calculated with these definitions range (for our test cases) between approximately −0.1 and +0.1 Ry. Consequently any quantity calculated with this or our choice of V^c is very similar in value as can be seen from Figs. 5, 6, and 9 below. One advantage of either definition, Eqs. (13)–(16), is that it can easily be extended to the case of complex lattices. A convenient extension of V^c based on the above equations is, however, less straightforward in the case of surfaces or interfaces as one optimal constant for all layers cannot be found when the potentials vary from layer to layer.[12]

The present "muffin-tin discontinuity" problem not only applies for spherically symmetric potentials (for ASA potentials it was already noted[13]), but due to the slowly converging shape functions, this might also be the case for full potentials that are not fully converged in L. It should be emphasized that full-potential methods not making use of the shape function technique such as the full-potential linearized aug-

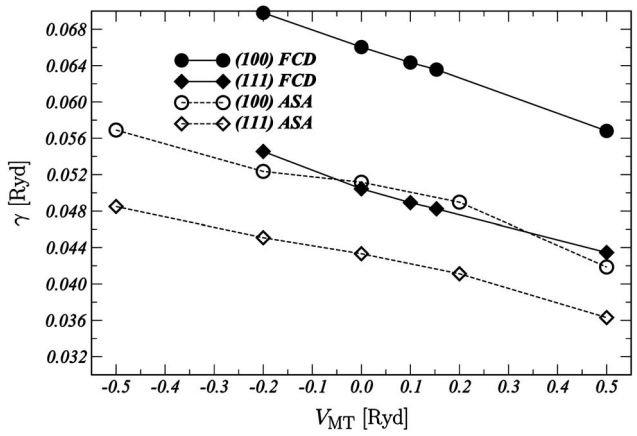

FIG. 6. Surface energies γ for (100) and (111) surfaces of Cu as calculated by using the FCD method and the ASA as a function of the potential at the muffin-tin radius, V_{MT}.

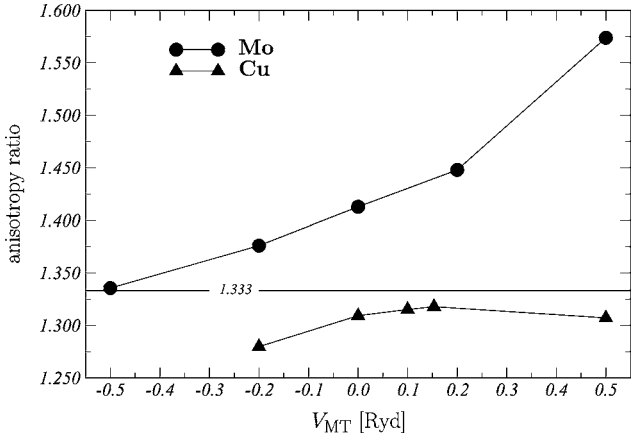

FIG. 7. Anisotropy ratio $\gamma(100)/\gamma(111)$ of Cu and Mo as a function of the potential at the muffin-tin radius, V_{MT}. The ideal value of 4/3 is indicated by the solid horizontal line.

mented plane-wave (FLAPW) method,[14,15] do not suffer from the problem discussed in this section.

IV. EVALUATION OF THE CHARGE DENSITY

At a given (complex) energy z the Green's function $G(z;\mathbf{r},\mathbf{r}')$ can be written in terms of spherical harmonics,

$$G(z;\mathbf{r},\mathbf{r}') = \sum_{LL'} Y_L(\hat{\mathbf{r}}_i) G^{ij}_{LL'}(z;r_i,r'_j) Y^*_{L'}(\hat{\mathbf{r}}'_j). \tag{17}$$

The radial part $G^{ij}_{LL'}(z;r_i,r'_j)$ can be expressed in terms of the regular and irregular scattering solutions of the spherically symmetric potential, $Z^i_\ell(z;r)$ and $J^i_\ell(z;r)$, respectively,

$$G^{ij}_{LL'}(z;r_i,r'_j) = Z^i_\ell(z;r_i)\tau^{ij}_{LL'}(z)Z^j_{\ell'}(z;r'_j) - J^i_\ell(z;r_>)Z^i_\ell(z;r_<)\delta_{ij}\delta_{LL'}, \tag{18}$$

where the $\tau^{ij}_{LL'}(z)$ denote the site angular momentum matrix elements of the scattering path operator[16] and $r_> = \max(r_i, r'_i)$ and $r_< = \min(r_i, r'_i)$.

The charge density is then defined as

$$\rho(\mathbf{r}) = -\frac{2}{\pi}\,\mathrm{Im}\int_{\cap} \mathrm{d}z G(z;\mathbf{r},\mathbf{r}), \tag{19}$$

where the energy integration, usually evaluated along a suitable contour in the upper complex semiplane, extends from the bottom of the valence band to the Fermi level and in the case of a nonrelativistic description a factor of 2 accounts for the spin degeneracy. Inserting Eq. (17) into Eq. (19) allows us to write the charge density confined to a cell labeled by i as follows:

$$\rho_i(\mathbf{r}_i) = -\frac{2}{\pi}\,\mathrm{Im}\sum_{LL'} Y_L(\hat{\mathbf{r}}_i) G_{i,LL'}(r_i) Y^*_{L'}(\hat{\mathbf{r}}_i) \tag{20}$$

$$= -\frac{1}{\pi\mathrm{i}}\sum_{LL'}[G_{i,LL'}(r_i) - G_{i,L'L}(r_i)^*] Y_L(\hat{\mathbf{r}}_i) Y^*_{L'}(\hat{\mathbf{r}}_i), \tag{21}$$

with

$$G_{i,LL'}(r_i) = \int_{\cap} \mathrm{d}z G^{ii}_{LL'}(z;r_i,r_i). \tag{22}$$

By using the identity

$$Y_L(\hat{\mathbf{r}}) Y^*_{L'}(\hat{\mathbf{r}}) = \sum_{L''} C^{L'}_{LL''} Y^*_{L''}(\hat{\mathbf{r}}), \tag{23}$$

the charge density can be expanded as

$$\rho_i(\mathbf{r}_i) = \sum_L \rho_{i,L}(r_i) Y^*_L(\hat{\mathbf{r}}_i), \tag{24}$$

with partial radial densities $\rho_{i,L}(r_i)$ being defined as

$$\rho_{i,L}(r_i) = -\frac{1}{\pi\mathrm{i}}\sum_{L'L''} C^{L''}_{LL'}[G_{i,L'L''}(r_i) - G_{i,L''L'}(r_i)^*]. \tag{25}$$

V. CALCULATION OF THE TOTAL ENERGY

A precise calculation of the total energy using first-principles electronic structure methods is crucial to obtain meaningful results for most bulk and surface properties. It is exactly the main advantage of the full-charge-density approximation to perform this step at the accuracy of full-potential methods. In this section we briefly outline the FCD scheme to calculate total energies for non-spin-polarized systems, an extension to the spin-polarized case being quite obvious.

Within density functional theory[10] the total energy $E_{\mathrm{tot}}[\rho]$ is defined by the sum of the kinetic energy $T[\rho]$, the electrostatic energy $U[\rho]$, and the exchange-correlation energy $E_{\mathrm{xc}}[\rho]$,

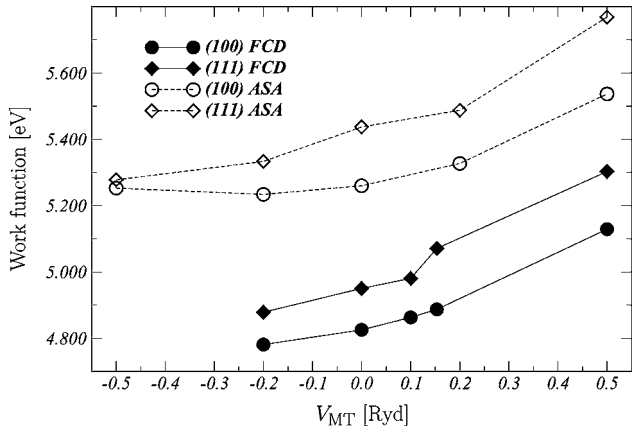

FIG. 8. Work functions for Cu(100) and Cu(111) as calculated by using the FCD method and the ASA as a function of the potential at the muffin-tin radius, V_{MT}.

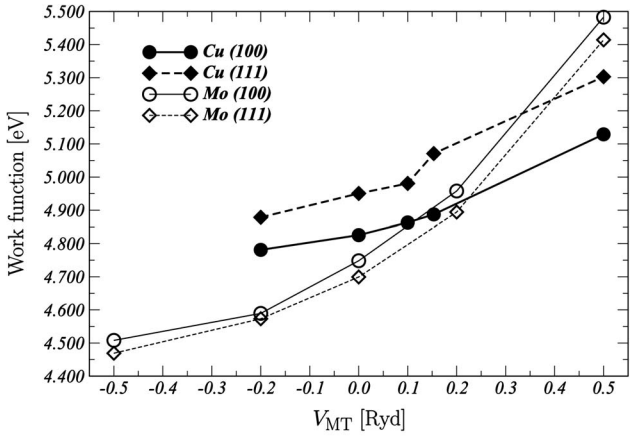

FIG. 9. Work functions for (100) and (111) surfaces of Cu and Mo as a function of the potential at the muffin-tin radius, V_{MT}.

$$E_{\mathrm{tot}}[\rho] = T[\rho] + U[\rho] + E_{\mathrm{xc}}[\rho]. \tag{26}$$

By using the Kohn-Sham equations the kinetic energy can be expressed as the sum of single-particle energies, containing core and valence band energy contributions E^{c} and E^{b}, respectively, and a "potential energy" E^{pot},

$$T[\rho] = E^{\mathrm{c}} + E^{\mathrm{b}} + E^{\mathrm{pot}}. \tag{27}$$

It should be noted that when calculating E^{pot} the same potential as the one that appears in the Kohn-Sham equations has to be used: namely the one defined in Eq. (10),

$$E^{\mathrm{pot}} = -\sum_i \int \mathrm{d}\mathbf{r}\rho(\mathbf{r})V(\mathbf{r})\sigma_i(\mathbf{r}) \tag{28}$$

$$= -\sum_i \int_0^{r_{i,\mathrm{BS}}} r_i^2 \mathrm{d}r_i \rho_{i,00}(r_i)V_{i,00}(r_i)\sigma_{i,00}(r_i), \tag{29}$$

where $r_{i,\mathrm{BS}}$ denotes the radius of the bounding sphere of the corresponding Wigner-Seitz polyhedron. Especially, this part of the kinetic energy has to be computed very accurately.

Following Weinert *et al.*[18] we calculate the electrostatic energy as

$$U[\rho] = \frac{1}{2}\sum_i \int_{\Omega_i} \mathrm{d}\mathbf{r}_i \rho_i(\mathbf{r}_i)\left(V_i^{\mathrm{c}}(\mathbf{r}_i) - \frac{2Z_i}{|\mathbf{r}_i|}\right) - \frac{1}{2}Z_i V_i^{\mathrm{c,Inter}}(\mathbf{0}), \tag{30}$$

where Z_i denotes the nuclear charge in cell i at $\mathbf{r}_i = \mathbf{0}$, while the Coulomb potential $V_i^{\mathrm{c}}(\mathbf{r}_i)$ is the sum of contributions from charge densities inside and outside the cell, $V_i^{\mathrm{c,intra}}(\mathbf{r}_i)$ and $V_i^{\mathrm{c,inter}}(\mathbf{r}_i)$, respectively,

$$V_i^{\mathrm{c}}(\mathbf{r}_i) = V_i^{\mathrm{c,intra}}(\mathbf{r}_i) + V_i^{\mathrm{c,inter}}(\mathbf{r}_i), \tag{31}$$

both of which have to be calculated up to an order of $2\ell_{\max}$ with respect to the expansion in Eq. (1). Note that, since in Eq. (28) only the $\ell = 0$ term of the Coulomb potential is used, within a full-charge-density scheme, Eqs. (28) and (30) cannot be combined in order to cancel the Coulomb singularities as suggested in Ref. 18. A particularly important contribution to the intercell potential arises from so-called near-field corrections (NFC's) which can efficiently be calculated by the so-called removed sphere method of Ref. 19 or the method discussed in Ref. 16. To obtain the intercell potential for bulk systems Ewald's method[20] is applied, while for surfaces and interfaces a method similar to that discussed by Kambe[21] is used.[16] In a recent publication[17] we have studied the convergence properties not only of the electrostatic energy but also of the electrostatic potential. For special test cases analytic expressions have been evaluated and for several $\ell_{\max}$ compared to the exact solution.

Finally, within the local density approximation the exchange-correlation energy

$$E_{\mathrm{xc}}[\rho] = \int \mathrm{d}\mathbf{r}\rho(\mathbf{r})\varepsilon_{\mathrm{xc}}[\rho(\mathbf{r})] \tag{32}$$

$$= \sum_i \int_0^{r_{i,\mathrm{BS}}} r_i^2 \mathrm{d}r_i \sum_{LL'L''} C^L_{L'L''}\rho_{i,L}(r_i)\varepsilon^{\mathrm{xc}}_{i,L'}(r_i)\sigma_{i,L''}(r_i), \tag{33}$$

$$\varepsilon^{\mathrm{xc}}_{i,L}(r_i) = \int \mathrm{d}\hat{\mathbf{r}}_i \varepsilon_{\mathrm{xc}}[\rho_i(\mathbf{r}_i)]Y_L(\hat{\mathbf{r}}_i)^*, \tag{34}$$

can be calculated by means of a direct Gaussian quadrature as described in Ref. 16.

VI. RESULTS

We first applied the FCD method described in Secs. II–V to calculate total energies and related properties for the bulk and the surface of Cu and Mo, both of them exhibiting fcc crystal structure. The core states were treated relativistically, while for the valence band we used the so-called scalar-relativistic approach.[16] For the exchange-correlation terms the functional of Ceperley and Alder[22] in the parametrization of Perdew and Zunger[23] was employed. In order to perform the necessary Brillouin zone integrals 45 k points have been used in the irreducible part of the two-dimensional Brillouin zone for the fcc(100) and 278 k points for the fcc(111) face.

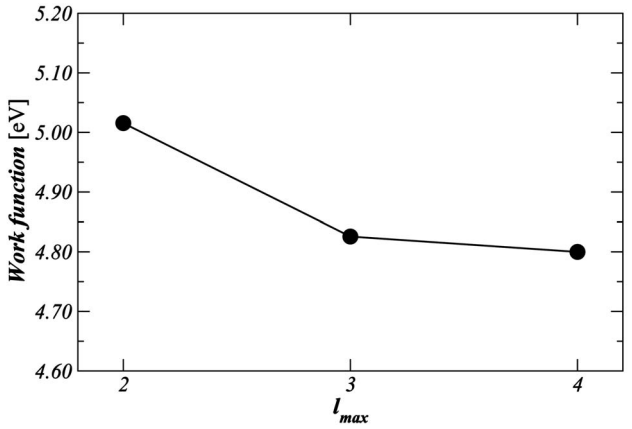

FIG. 10. Angular momentum convergence of the work function of fcc Cu(100) as calculated using the FCD scheme using $V_{MT}=0$.

In all cases 16 energy points have been used on a complex semicircular contour such that the density of points is increased as the Fermi energy is approached. For the bulk systems we determined the equilibrium lattice constants; for the surface calculations, however, we used experimental lattice constants for all cases under consideration. The angular momentum quantum number for the scattering solutions was $\ell_{max}=3$; hence, in the calculation of the total energy the potential and charge density were expanded up to $\ell_{max}=6$. To calculate the surface energy γ, we evaluated the difference between the total energy per unit cell of the self-consistently treated surface region of N_a atomic layers and N_{vac} vacuum layers and N_a times the total energy/unit cell in the bulk:

$$\gamma = E_{tot}^{surf}(N_a + N_{vac}) - N_a E_{tot}^{bulk}. \quad (35)$$

We carefully checked the convergence of the results with respect to the number of self-consistently treated surface and vacuum layers; see Ref. 5. It was found that $N_a=10$ and $N_{vac}=2$ completely serve the purpose and hence have been used for all systems under investigation.

In particular, we focused on the dependence of the results with respect to the potential shift as discussed in Sec. III and as parametrized by the value of the potential at the muffin-tin radius, V_{MT}. For the (simple lattice) bulk case it is trivial to impose this constraint since each cell potential is identical. For the surface calculations we used this potential shift as a bulk boundary condition for the Poisson equation to be solved for the intercell Coulomb potential; see Ref. 16. The surface potentials were then self-consistently adjusted to the specific potential shift.

A. Bulk properties

For fixed lattice parameters $a_{Cu}=6.831$ a.u. and $a_{Mo}=7.656$ a.u., the dependence of the total energy on V_{MT} is shown in Fig. 3. In addition, the corresponding results from an ASA calculation are also displayed in the case of Cu. In all cases, the variation of E_{tot} is within some tenths of rydbergs; the displayed curves show a maximum for quite different values of V_{MT}. A physical relevance can, however, hardly be associated with this behavior.

In Fig. 4 the total energy of bulk Cu is displayed for different values of V_{MT} as a function of the fcc lattice constant. According to Fig. 3 the total energies differ considerably with respect to V_{MT}; however, each of the curves exhibits a minimum at approximately the same lattice constant, $a_0(V_{MT})$ (see Fig. 5). As can be inferred from this figure, in the range of V_{MT} under consideration the calculated equilibrium lattice constant changes less than 0.03 a.u.—i.e., is of a relative accuracy of 0.5%. Choosing an optimal value for V_{MT}—namely, $V_{MT}=0$ (see Sec. III)—the local density-approximation (LDA) equilibrium lattice constant for Cu can be deduced to be $a_0=6.70\pm0.02$ a.u. The calculated bulk modulus B is also plotted in Fig. 5 and, as can be seen, shows a weak dependence with respect to V_{MT}. Interestingly, in the vicinity of $V_{MT}=0$ an almost stationary behavior of $B(V_{MT})$ can be seen. Therefore, we deduce a LDA value of $B=1.65\pm0.01$ Mbar for Cu.

Quite surprisingly, our calculated lattice parameter and bulk modulus for Cu compare better to the experimental values of 6.84 a.u. and 1.37 Mbar than those calculated in terms of a FP-KKR-LDA or a FLAPW-LDA method, 6.63 a.u and 1.88 (1.90) Mbar,[24] respectively. It should be noted that by using the generalized gradient approximation (GGA) for the exchange-correlation functional the FP-KKR method produced an almost perfect agreement with experiment.[24]

B. Surface properties

Taking the experimental lattice constants and neglecting surface relaxations we first performed calculations for Cu(100) and Cu(111) surfaces. In Fig. 6 the corresponding surface energies γ as obtained from the present FCD method and by using the ASA are shown as a function of V_{MT}. As can be inferred, the calculated surface energies are more sensitive to V_{MT} than the bulk equilibrium lattice constants or bulk moduli, since they vary about 10% in magnitude for $-0.5\ \text{Ry} < V_{MT} < 0.5\ \text{Ry}$. The FCD surface energies at $V_{MT}=0$ of 0.90 eV for Cu(100) and 0.69 eV for Cu(111), however, compare well to those calculated by the FP-KKR, 0.87 eV and 0.67 eV,[25] the FLAPW, 0.81 eV and 0.62 eV,[25]or the FCD-LMTO method, 0.91 eV and 0.71 eV,[26] respectively.

In Ref. 25 a "broken-bond rule" for the surface of noble metals has been proposed. According to this rule the anisotropy ratio, defined as $\gamma(100)/\gamma(111)$, is close to the ideal value of 4/3 as follows from the number of nearest neighbors of atoms in the top surface layers. In Fig. 7 this anisotropy ratio is plotted for Cu and Mo as a function of V_{MT}. For Cu a weak dependence of this quantity on V_{MT} is observed, and the value of 1.31 for $V_{MT}=0$ agrees nicely with other values reported in the literature.[25,26] For Mo the anisotropy ratio depends more strongly on V_{MT} ranging from 1.34 at $V_{MT}=-0.5$ Ry to 1.57 at $V_{MT}=0.5$ Ry. It should be noted that this nearest-neighbor broken-bond rule is less applicable in the case of Mo because of the larger spatial extent of the open-shell 4*d* orbitals.

It is worthwhile to consider the calculated work functions that, as can be seen from Fig. 8 in the case of Cu, are sig-

TABLE I. Calculated surface energies, anisotropy ratios, and work functions for some transition metals. All calculations are for fcc lattices using the experimental lattice constants. In all cases the bulk potential has been shifted to zero at the muffin-tin radius.

		γ (eV/atom)		$\gamma(100)/\gamma(111)$	Work function (eV)	
Cu	(100)	0.899	0.87,[a] 0.906,[b] 0.81[c]	1.309	4.826	
	(111)	0.686	0.67,[a] 0.707,[b] 0.62[c]		4.951	
Mo	(100)	1.794		1.413	4.748	
	(111)	1.270	1.36[d]		4.699	4.98,[e] 4.65[d]
Pd	(100)	1.102	1.049,[a] 1.152[b]	1.283	5.504	
	(111)	0.859	0.822,[a] 0.824[b]		5.419	5.53,[e] 5.33[d]
Ag	(100)	0.757	0.73,[a] 0.653,[b] 0.65[c]	1.327	4.564	
	(111)	0.571	0.57,[a] 0.583,[b] 0.51[c]		4.575	4.67,[e] 4.56[d]
Pt	(100)	1.371	1.272,[a] 1.378[b]	1.368	6.401	
	(111)	1.002	0.957,[a] 1.004[b]		6.137	
Au	(100)	0.859	0.84,[a] 0.895,[b] 0.68[c]	1.325	5.637	
	(111)	0.648	0.62,[a] 0.611,[b] 0.50[c]		5.526	

[a]FP-KKR calculations, Ref. 25.
[b]FCD-LMTO calculations, Ref. 26.
[c]FLAPW calculations, Ref. 25.
[d]FCD-LMTO calculations, Ref. 1.
[e]FP-LMTO calculations, Ref. 27.

nificantly reduced by the FCD scheme as compared to the ASA, a fact that was already noticed about 10 years ago, when introducing the FCD method in Ref. 1. In particular, for Mo a variation of about 10% with respect to V_{MT} of the calculated work function can be established from Fig. 9. In addition Fig. 10 illustrates the convergence of the work function in the case of Cu(100) as a function of $\ell_{\max}$ used in the solution of the radial equations.

Finally, in Table I we summarized the surface energies and the work functions for some transition metals obtained by using the presently applied FCD-SKKR method. For all these calculations the bulk potentials have been shifted to zero at the muffin-tin radius. A comparison with other FP and FCD values from the literature, also listed in Table I, indicates that the method introduced and applied in this paper is capable of yielding results with an accuracy of today's computational standards set by FP *ab initio* approaches.

VII. CONCLUSIONS

A full-charge-density version of the SKKR method has been presented. It relies on making use of only a spherically symmetric potential while still keeping all components in the expansion of the charge density. The major improvement over the ASA is the much more accurate evaluation of the total energy and the exact solution of Poisson's equation.

It turns out that for both the ASA and FCD methods a dependence on a numerical parameter—the potential shift—is present. For bulk properties such as the equilibrium lattice constant and the bulk modulus this dependence is found to be of minor importance, while for the surface energies and work functions a much larger sensitivity was found.

Based on experiences made so far it is hard to answer the question whether for FCD calculations there is a certain value of the potential shift which for any physical or numerical reason has to be preferred over others. Figure 2 suggests that the best choice one can make in a (simple lattice) bulk calculation is to shift the potential to zero at the muffin-tin radius, as there the difference between the full-crystal potential and the individual single-site potentials is minimized. However, even for a bulk system with sublattices this choice can be made at best in terms of an average over nonequivalent potentials. Furthermore, in the case of surfaces the (layer resolved) potentials are shifted upwards until they reach the vacuum potential level. Thus probably a different choice for the potential shift can turn out to be optimal. Still, it seems that it is more favorable to shift the potential rather to positive values at and beyond the muffin-tin radius not only for this particular reason, but also because the energy-dependent KKR structure constants show better convergence properties in this regime.

It has to be emphasized that the main reasons to use the FCD-SKKR method are that (1) truly semi-infinite systems can be studied, (2) an implementation of fully relativistic spin-polarized descriptions[16] are rather straightforward, and (3) even a Green's function corresponding to a full potential for evaluating physical properties can be obtained. In particular by avoiding a film geometry mandatory—e.g., in the FLAPW method in the case of systems with surfaces or interfaces—a more realistic description of the substrate can be achieved. Clearly enough also the possibility of using an approach based on the Dirac equation rather than applying a perturbative treatment of spin-orbit coupling offers advantages in dealing with magnetic anisotropies. Therefore, the present paper has to be viewed also with this respect, rather than describing only well-known physical properties such as equilibrium lattice constants, bulk moduli, or surface energies. This is necessary only once in order to gauge the numerical reliability of results to be obtained.

ACKNOWLEDGMENTS

Financial support was provided by the Center for Computational Materials Science (Contract Nos. Zl.98.366 and GZ 45.547), the Hungarian Research and Technological Innovation Council and the Bundesministerium für Auswärtige Angelegenheiten of Austria (Contract No. A-3/03), and the Hungarian National Scientific Research Foundation (Contract Nos. OTKA T037856 and T046267).

[1] L. Vitos, J. Kollár, and H. L. Skriver, Phys. Rev. B **49**, 16694 (1994).
[2] L. Vitos and J. Kollár, Phys. Rev. B **51**, 4074 (1995).
[3] L. Vitos, J. Kollár, and H. L. Skriver, Phys. Rev. B **55**, 13521 (1997).
[4] L. Vitos, H. L. Skriver, B. Johansson, and J. Kollár, Comput. Mater. Sci. **18**, 24–38 (2000).
[5] L. Szunyogh, B. Újfalussy, P. Weinberger, and J. Kollár, Phys. Rev. B **49**, 2721 (1994).
[6] Note that the complex spherical harmonics are defined as

$$Y_{\ell m}(\theta,\varphi) = C_{\ell m} P_\ell^{|m|}(\cos\theta) e^{im\varphi},$$

$$C_{\ell m} = \mathrm{i}^{m+|m|} \sqrt{\frac{2\ell+1}{4\pi} \frac{(\ell-|m|)!}{(\ell+|m|)!}},$$

with $P_\ell^{|m|}(\cos\theta)$ being the associated Legendre functions.
[7] N. Stefanou, H. Akai, and R. Zeller, Comput. Phys. Commun. **60**, 231 (1990).
[8] N. Stefanou and R. Zeller, J. Phys.: Condens. Matter **3**, 7599 (1991).
[9] Yang Wang, G. M. Stocks, and J. S. Faulkner, Phys. Rev. B **49**, 5028 (1994).
[10] W. Kohn and L. J. Sham, Phys. Rev. **140**, A1133 (1965).
[11] L. Vitos, Phys. Rev. B **64**, 014107 (2001).
[12] J. Kollár, L. Vitos, and K. Kádas (private communication).
[13] R. Hammerling, Ph.D. thesis, Vienna University of Technology, 2003.
[14] H. Krakauer, M. Posternak, and A. J. Freeman, Phys. Rev. B **19**, 1706 (1979).
[15] E. Wimmer, H. Krakauer, M. Weinert, and A. J. Freeman, Phys. Rev. B **24**, 864 (1981).
[16] J. Zabloudil, R. Hammerling, L. Szunyogh, and P. Weinberger, *Electron Scattering in Solid Matter* (Springer, Berlin, 2004).
[17] R. Hammerling, J. Zabloudil, L. Szunyogh, and P. Weinberger, Philos. Mag. **86**, 25 (2006).
[18] M. Weinert, E. Wimmer, and A. J. Freeman, Phys. Rev. B **26**, 4571 (1982).
[19] D. M. C. Nicholson and W. A. Shelton, J. Phys.: Condens. Matter **14**, 5601 (2002).
[20] P. P. Ewald, Ann. Phys. (Leipzig) **64**, 253 (1921).
[21] K. Kambe, Z. Naturforsch. A **22**, 322 (1967); **22**, 422 (1967); **23**, 1280 (1968).
[22] D. M. Ceperley and B. J. Alder, Phys. Rev. Lett. **45**, 566 (1980).
[23] J. P. Perdew and A. Zunger, Phys. Rev. B **23**, 5048 (1981).
[24] N. Papanikolaou, R. Zeller, and P. H. Dederichs, J. Phys.: Condens. Matter **14**, 2799 (2002).
[25] I. Galanakis, G. Bihlmayer, V. Bellini, N. Papanikolaou, R. Zeller, S. Blügel, and P. H. Dederichs, Europhys. Lett. **58**, 751 (2002); I. Galanakis, N. Papanikolaou, and P. H. Dederichs, Surf. Sci. **1**, 511 (2002).
[26] L. Vitos, A. V. Ruban, H. L. Skriver, and J. Kollár, Surf. Sci. **411**, 186 (1998).
[27] M. Methfessel, D. Hennig, and M. Scheffler, Phys. Rev. B **46**, 4816 (1992).